Characterizing Surface Ice-philicity Using Molecular Simulations and Enhanced Sampling

Sean M. Marks,[†,‡] Zachariah Vicars,[†,‡] Aniket U. Thosar,[†] and Amish J. Patel[*,†]

†Department of Chemical and Biomolecular Engineering, University of Pennsylvania

‡S.M.M. and Z.V. contributed equally to this paper

E-mail: amish.patel@seas.upenn.edu

1

Abstract

The formation of ice, which plays an important role in diverse contexts, ranging from cryopreservation to atmospheric science, is often mediated by solid surfaces. Although surfaces that interact favorably with ice (relative to liquid water) can facilitate ice formation by lowering nucleation barriers, the molecular characteristics that confer a surface with "ice-philicity" are complex and incompletely understood. To address this challenge, here we introduce a robust and computationally efficient method for characterizing surface ice-philicity, which combines molecular simulations and enhanced sampling techniques to quantify the free energetic cost of increasing surface-ice contact at the expense of surface-water contact. Using this method to characterize the ice-philicity of a family of model surfaces that are latticed matched with ice but vary in their polarity, we find that the non-polar surfaces are moderately ice-phobic, whereas the polar surfaces are highly ice-philic. In contrast, for surfaces that display no complementarity to the ice lattice, we find that ice-philicity is independent of surface polarity and that both non-polar and polar surfaces are moderately ice-phobic. Our work thus provides a prescription for quantitatively characterizing surface ice-philicity and sheds light on how ice-philicity is influenced by lattice matching and polarity.

Introduction

The freezing of water into ice is a ubiquitous process that is important in diverse fields, ranging from cryobiology to atmospheric science.[1,2] Although large nucleation barriers impede the formation of ice at low to moderate supercooling, solid surfaces that interact favorably with ice can lower those barriers. Surfaces of various organic or inorganic materials, such as graphite or clay minerals, which utilize different chemical and topological features to interact with ice,[3–5] can facilitate the heterogeneous nucleation of ice to an extent that depends on their preference for ice over liquid water, i.e. on the ice-philicity of the surface. Conversely, a surface that is ice-phobic resists the formation of ice, and could serve as the basis for

designing ice-repellant surface coatings.[6–9] Thus, being able to characterize and understand surface ice-philicity/phobicity is the key to both facilitating and inhibiting ice formation. To this end, a variety of experimental techniques, based on scattering, spectroscopy and microscopy, have been used to estimate the rates of heterogeneous ice nucleation;[10–18] the molecular characteristics of surface that enable it to promote or inhibit ice formation remain poorly understood.

Computational studies are well-suited to uncovering the molecular underpinnings of surface ice-philicity, but the typical timescales that are accessible to molecular simulations are roughly six orders of magnitude smaller than those in the experiments. Consequently, simulation studies have focused on the deep supercooling regime or highly ice-philic surfaces, which are expected to result in relatively small heterogeneous nucleation barriers. For example, Michaelides and co-workers[19–21] used long molecular dynamics (MD) simulations to study heterogeneous ice nucleation at temperatures well below the melting point. Correspondingly, to interrogate whether certain surfaces are excellent ice nucleators, Fraux and Doye[22] as well as Glatz and Sarupria[23] performed simulations near the melting temperature (low supercooling), and observed whether the surfaces were able to nucleate ice. These approaches have provided valuable insights into how the molecular characteristics of a surface influence their ability to nucleate ice;[24,25] however, their classification of surfaces as good or bad ice nucleators can depend on certain choices, such as simulation temperature and time.

To provide a more quantitative measure of surface ice-philicity, Molinero and co-workers[26–28] systematically cooled water below its melting temperature and obtained the non-equilibrium freezing temperature at which a surface nucleates ice. The forward flux sampling (FFS) technique, which provides quantitative estimates of ice nucleation rates,[29–34] but is much more computationally expensive than the above approaches, has also been used to characterize the propensity of select surfaces to nucleate ice. Finally, Espinosa et al.[35] and Pedevilla et al.[36] introduced a seeding method, wherein the growth rate of a pre-formed ice nucleus (or seed) of a particular size and shape, which is in contact with the surface, is used to study

3

heterogeneous nucleation.

In this paper, we introduce a computationally efficient technique for robustly and unambiguously characterizing the thermodynamic preference of a surface for ice over liquid water, i.e., surface ice-philicity. The technique involves biasing the number of ice-like waters adjacent to the surface of interest to systematically increase surface-ice contact at the expense of surface-water contact, and computing the corresponding free energy. To demonstrate this technique, we characterize the ice-philicity of a family of model surfaces with varying polarities and perfect lattice-match with ice. We find that ice-philicity increases with surface polarity, with non-polar surfaces being moderately ice-phobic and polar ones being highly ice-philic. We also study surfaces that display no particular complementarity with the structure of ice and find their ice-philicity does not depend on polarity; both polar and non-polar surfaces are moderately ice-phobic. Our work thus provides a prescription for quantifying surface ice-philicity, and highlights the importance of both lattice-matching and polarity in conferring surfaces with ice-philicity; it also suggests different strategies for designing ice-phobic surfaces.

Methods

Theory

To characterize the ice-philicity of a surface, i.e. its preference for ice over liquid water, here we generalize the "Surface Wetting and Interfacial Properties using Enhanced Sampling" (SWIPES) method, which was introduced in ref. 37 for characterizing surface hydrophobicity. To this end, we employ the process, shown in Fig. 1, at a fixed temperature, T, which is not necessarily equal to the melting temperature, T_m, of ice. As the system goes from state $\mathcal{A}$ to state $\mathcal{B}$, a certain number of water molecules, $\Delta\lambda$, transform from liquid water to ice. Correspondingly, the ice-water interface advances by a distance ΔH, while retaining its shape, as predicted by interfacial thermodynamics and shown in ref. 37. The system also
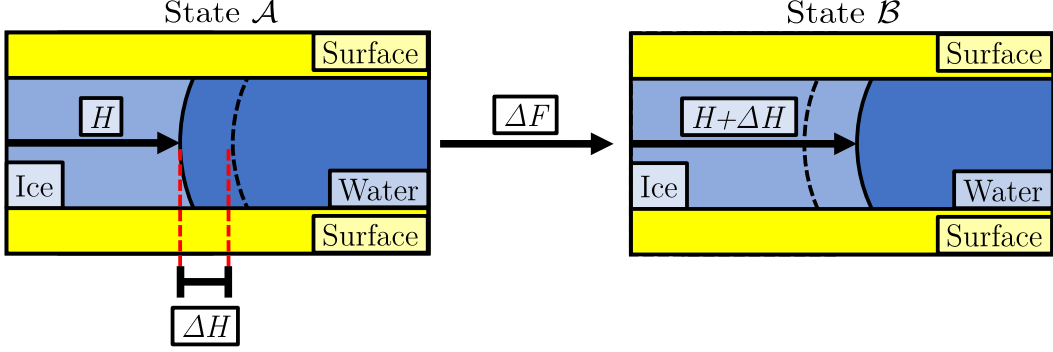
Figure 1: Schematic illustrating SWIPES. The solid surface of interest is shown in yellow, ice in light blue, and liquid water in dark blue. The location of the ice-water interface, H, is shown at the midpoint between the solid surfaces. In going from state $\mathcal{A}$ to state $\mathcal{B}$, the ice-liquid interface advances by a distance, ΔH, and the system free energy changes by ΔF.

exchanges a certain amount of surface-water contact area, ΔA_S, for an equivalent amount of surface-ice contact area. During this process, the free energy of the system changes by:

$$\Delta F = \left(\gamma_\mathrm{SI} - \gamma_\mathrm{SL}\right)\Delta A_\mathrm{S} + \mu_\mathrm{fr}\Delta\lambda = \left(-k\gamma_\mathrm{IL}\right)(2\Delta H L) + \mu_\mathrm{fr}\Delta\lambda \tag{1}$$

where γ_SI and γ_SL are the surface tensions associated with the surface-ice and surface-liquid interfaces, respectively; μ_fr is the chemical potential difference between ice and liquid water; $k \equiv \left(\gamma_\mathrm{SL} - \gamma_\mathrm{SI}\right)/\gamma_\mathrm{IL}$ is the wetting coefficient that characterizes the relative preference of the surface for ice over water; γ_IL is the ice-water surface tension; and L is the length of the system into the page.

The wetting coefficient, k, is the thermodynamic measure of surface ice-philicity we wish to obtain; for ice-philic surfaces, $k > 0$, whereas for ice-phobic surfaces, $k < 0$. Moreover, the magnitude of k must be less than unity, i.e., $-1 \leq k \leq 1$, and according to Young's equation, $k = \cos\theta$, where θ is the contact angle that an ice nucleus, which is surrounded by liquid water, adopts when it is in contact with the surface.[38] Rearranging Eqn. 1, we obtain:

$$k\gamma_\mathrm{IL} = -\frac{1}{2L}\frac{\Delta F - \mu_\mathrm{fr}\Delta\lambda}{\Delta H}. \tag{2}$$

Eqn. 2 highlights that by estimating ΔF, ΔH, and $\Delta\lambda$ for a surface of interest, we can obtaining a quantitative measure of its ice-philicity (assuming that the surface-independent quantities μ_{fr} and γ_{IL} are known). Conversely, by employing a surface with a known value of k, this approach can also be used to estimate the ice-water surface tension, γ_{IL}. Moreover, because the above process can be performed at any temperature, T (and not just T_{m}), γ_{IL} and k can be readily obtained under supercooled (or superheated) conditions.

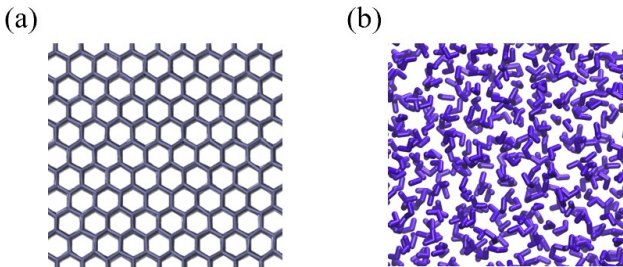## Model Surfaces

(a) (b)

Figure 2: Model surfaces for exploring ice-philicity. (a) The pseudo-ice family of surfaces is created by restraining the oxygens of ice I_h to their lattice sites, and scaling the surface polarity by a constant factor, α, yielding surfaces with perfect lattice match to ice. (b) The pseudo-water family of surfaces is similarly constructed by position restraining a slab of liquid water to yield surfaces with varying polarity but no particular complementarity with the lattice of ice.

To understand how the molecular characteristics of a surface influence its ice-philicity, we designed two families of model surfaces. The "*pseudo-ice*" family of surfaces are comprised of a 2 nm slab of hexagonal ice (ice I_h) with its water oxygens restrained to their lattice sites (Fig. 2a); the spring constant for the harmonic restraining potentials is chosen to be 40000 kJ/mol/nm^2 so that the variance of surface atom positions is roughly an order of magnitude smaller than that in bulk hexagonal ice. Thus, all the pseudo-ice surfaces are perfectly lattice-matched with ice. However, the surfaces differ in their polarity, which is varied by scaling the partial charges of the surface atoms by a factor, α, between 0 and 1. Our pseudo-ice surfaces are constructed to interact with their hydration waters

6

through their basal planes. However, given the similarity in the surface tensions of the basal and prism planes,[35] we expect pseudo-ice surfaces constructed using other crystal planes to behave in similar ways. To investigate the influence of lattice matching (or lack thereof) on ice-philicity, we designed a complementary family of "*pseudo-water*" surfaces by similarly position-restraining the oxygen atoms in a 2 nm slab of liquid water (drawn from a configuration at 298 K and 1 bar, Fig. 2b). The resulting surfaces resemble liquid water in their local ordering and lack the long-range order found in ice. Once again, the family of pseudo-water surfaces with a range of polarities is obtained by systematically scaling the partial charges of the surface atoms by $0 \leq \alpha \leq 1$.
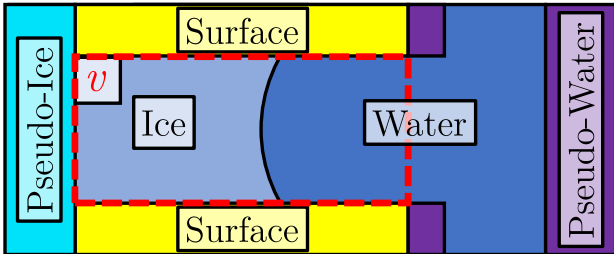
Simulation Setup

Figure 3: Illustrating boundary surfaces and end-caps in the SWIPES simulation setup. The simulation setup features a pseudo-ice boundary wall with $\alpha = 1$ (cyan) and a pseudo-water boundary wall with $\alpha = 1$ (purple) to ensure that ice grows from left to right in the region, v (red dashed box), between the surfaces of interest (yellow). Pseudo-water end-caps with $\alpha = 1$ (purple) are also used to prevent ice-philic surfaces from structuring the waters at the (right) ends of the surfaces.

Fig. 3 illustrates the SWIPES simulation setup used for characterizing the ice-philicity of the pseudo-ice and pseudo-water surfaces. We place a 1 nm thick slab of pseudo-ice with $\alpha = 1$ at the left end of the solid surfaces of interest to break translational symmetry and facilitate ice growth in v from left to right. We similarly place a 1 nm thick slab of pseudo-water ($\alpha = 1$) to ensure that the right side of v is occupied by liquid water. Finally, to prevent our surfaces of interest from structuring or freezing water outside v, we placed two pseudo-water end-caps to their right. The simulation box dimensions were approximately

12.1 nm, 5.9 nm, and 3.636 nm in the x, y, and z directions, respectively. Apart from the molecules comprising the surfaces of interest, the boundary slabs and the end-caps described above, the simulation box contained 4840 mobile water molecules that are free to be in the liquid water or ice phases.

Simulation Details

Molecular dynamics simulations were performed using a version of GROMACS 2016.3 that was suitably modified to exercise control over the number of ice-like waters in an observation volume of interest. Simulations were performed using the leapfrog integrator with a time-step of 2 fs. The mobile water molecules were constrained using the SETTLE algorithm,[39] whereas waters belonging to the pseudo-water and pseudo-ice surfaces were constrained using LINCS.[40] Pseudo-ice surfaces were generated using the GenIce package,[41] and the surfaces were solvated using the Packmol package[42] to generate initial configurations, which were then subject to energy minimization. The stochastic velocity rescale thermostat[43] with a time constant of 0.5 ps was used for temperature coupling, and the majority of our simulations were performed at 298 K to avoid slower dynamics and longer correlation times at lower temperatures. The Berendsen barostat[44] was used for equilibration and to obtain the initial configuration used in the SWIPES simulations, whereas the Parrinello-Rahman barostat[45] was used for production runs. Anisotropic pressure coupling was used in the x and y directions to allow the system to respond to changes in density as parts the system freeze/melt and to prevent the build-up of stress on the ice lattice. A cutoff distance of 1 nm was used for Lennard-Jones and short-ranged electrostatic interactions. Long-ranged electrostatic interactions were treated using the particle-mesh Ewald (PME) method.[46] The TIP4P/Ice water model was chosen because it captures several properties of ice and liquid water, such as density, freezing temperature, enthalpy of fusion and surface tension.[47]

Exercising control over ice formation

To control the extent to which ice wets the solid surface in our simulations, we bias an order parameter, q_v that acts in the region, v, between the surfaces of interest; q_v must be capable of distinguishing liquid-like and ice-like water within v. In particular, we apply a harmonic biasing potential $\mathcal{U}_{\mathrm{b}}^{(\kappa, q^*)}(q_v) = \frac{1}{2}\kappa(q_v - q^*)^2$. The value q^* defines a set-point for the desired amount of ice in the system and the magnitude of κ controls how tightly bound q_v is to q^*. A schematic of how increasing q^*, and thereby the value of q_v sampled, affects the extent to which the surface is wet by ice is shown in Fig. 4.
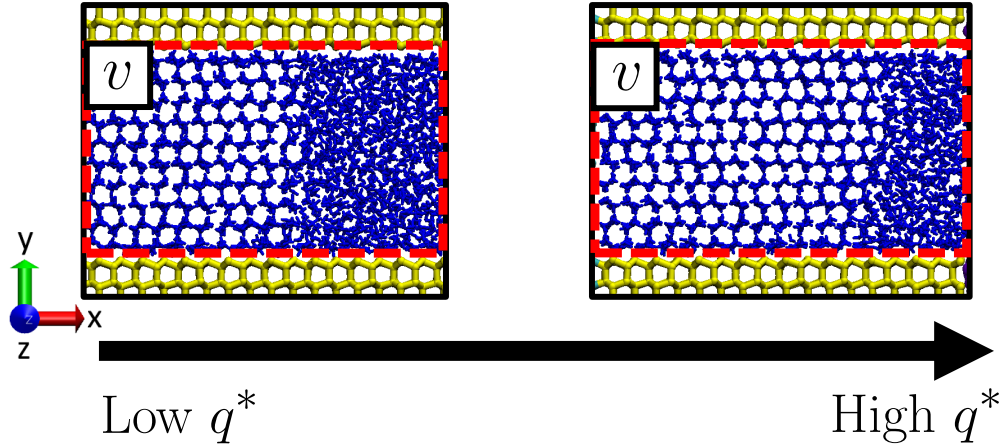

Figure 4: To control the extent to which ice wets the surfaces (yellow), we apply a harmonic biasing potential, $\frac{\kappa}{2}(q_v - q^*)^2$, that acts on an order parameter, q_v, which is capable of discriminating between liquid-like and ice-like waters in v (red dotted line). Waters are shown in blue.

Assuming that the two states shown in Fig.1 correspond to biasing parameters q^* and $q^* + \mathrm{d}q^*$, respectively (with κ fixed), the free energy difference between these states is $\mathrm{d}F_{\kappa,q^*} = F_{\kappa,q^*+\mathrm{d}q^*} - F_{\kappa,q^*}$. Correspondingly, the ice-liquid interface advances by $\mathrm{d}\langle H \rangle_{\kappa,q^*} \equiv \langle H \rangle_{\kappa,q^*+\mathrm{d}q^*} - \langle H \rangle_{\kappa,q^*}$, and the volume v contains $\mathrm{d}\langle \lambda_v \rangle_{\kappa,q^*} \equiv \langle \lambda_v \rangle_{\kappa,q^*+\mathrm{d}q^*} - \langle \lambda_v \rangle_{\kappa,q^*}$ additional ice-like waters, where $\langle \mathcal{A} \rangle_{\kappa,q^*}$ denotes the average value of observable $\mathcal{A}$ in the biased ensemble with fixed κ and q^*. Defining $f_q \equiv \frac{\mathrm{d}F_{\kappa,q^*}}{\mathrm{d}q^*}$, $h_q \equiv \frac{\mathrm{d}\langle H \rangle_{\kappa,q^*}}{\mathrm{d}q^*}$, and $s_q \equiv \frac{\mathrm{d}\langle \lambda_v \rangle_{\kappa,q^*}}{\mathrm{d}q^*}$, eqn. 2 can then be written as:

$$k\gamma_{\mathrm{IL}} = -\frac{1}{2L}\frac{f_q - s_q\mu_{\mathrm{fr}}}{h_q}. \tag{3}$$

9

Importantly, as discussed in ref. 37, s_q, h_q, and f_q are expected to be independent of q^*. In particular, for a judiciously chosen order parameter, the number of ice-like waters should grow linearly with q^*, resulting in a constant s_q. Moreover, because the interface position varies linearly with the ice-like waters in the system, h_q should also be a constant. Finally, according to eq. 3, if s_q and h_q are independent of q^*, then f_q must also be constant.

Estimating f_q

The free energy slope, f_q, can by readily obtained by estimating the average, $\langle q_v \rangle_{\kappa,q^*}$, in the biased ensemble. In particular, using the thermodynamic integration formula,[37,48] we obtain:

$$f_q = \frac{\mathrm{d}F_{\kappa,q^*}}{\mathrm{d}q^*} = \left\langle \frac{d\mathcal{U}_{\mathrm{b}}^{(\kappa,q^*)}}{dq^*} \right\rangle_{\kappa,q^*} = -\kappa\left(\langle q_v \rangle_{\kappa,q^*} - q^*\right) \tag{4}$$

Because f_q is expected to be independent of q^*, we expect $\langle q_v \rangle_{\kappa,q^*}$ to be a linear function of q^* with unit slope and an intercept that is equal to $-f_q/\kappa$. We thus use the intercept obtained from a linear fit of $\langle q_v \rangle_{\kappa,q^*}$ vs. q^* to estimate f_q.

Estimating h_q

To determine how the ice-liquid interface moves with increasing q^*, we estimate the position of the interface, H, for every configuration in our biased simulations. To this end, we first classify each water i as being ice-like or liquid-like by using an indicator function, $\tilde{h}_{\mathrm{ice}}(i)$, which relies on the order parameter, $\bar{q}_6(i)$, proposed by Lechner and Dellago;[49] the functional form of $\tilde{h}_{\mathrm{ice}}(i)$ is described in detail in sec. S1 of the SI. We then compute the one-dimensional ice density profile along the x-direction as:

$$\tilde{\rho}_{\mathrm{ice}}(x) = \frac{1}{L_y L_z} \sum_{i=1}^{N_w} \tilde{h}_{\mathrm{ice}}(i)\phi(x - x_i), \tag{5}$$

where $\phi(x)$ is a coarse-graining function that "smears out" the location of particle i,[50] and it is chosen to be a Gaussian that has a width of 0.3 nm, and is truncated and shifted down

at 0.6 nm.[51] For every simulation snapshot, we then obtain the location of the ice-water interface, H, by fitting $\tilde{\rho}_{\text{ice}}(x)$ to the sigmoidal function, $a \cdot \tanh\left[b \cdot (x - H)\right] + c$, with H, a, b, and c being the fit parameters. The slope of $\langle H \rangle_{\kappa, q^*}$ as a function of q^* then provides h_q.

Estimating s_q

To quantify the increase in the average number of ice-like waters, $\langle \lambda_v \rangle_{\kappa, q^*}$, with q^*, we recognize that $\langle \lambda_v \rangle_{\kappa, q^*}$ increases proportionally with $\langle H \rangle_{\kappa, q^*}$. Correspondingly, s_q is proportional to h_q with the proportionality constant being approximately equal to $L_z W \rho_{\text{ice}}$, where W is the separation between the surfaces and ρ_{ice} is the bulk density of ice. The proportionality constant can also be estimated more precisely by averaging the number of ice-like waters in a slab of unit thickness, as described in detail in sec. S2 of the SI.

Estimating μ_{fr}

To compute μ_{fr}, we use the interface pinning method,[52] which employs a simulation setup that is quite similar to SWIPES, with the primary distinction being the absence of a surface (as well as any boundary slabs or end-caps). As shown in sec. S3 of the SI, we obtain the value of μ_{fr} at 298 K to be 0.54 ± 0.1 kJ/mol.

Choosing the Order Parameter, q_v

To perform the SWIPES calculations proposed above, we must bias an order parameter that is capable of discriminating between liquid water and ice. Although several such order parameters have been proposed[49,53] most of them are either discontinuous or non-differentiable functions of particle positions, making them challenging to bias in conjunction with molecular dynamic simulations. Here, we circumvent this challenge through the use of coarse-grained indicator functions .[51,54] In particular, as our primary order parameter of choice, we choose

the approximate number of ice-like molecules, $\tilde{M}_v$, in v, which is defined as:

$$\tilde{M}_v = \sum_{i=1}^{N_{\mathrm{w}}} \tilde{h}_{\mathrm{ice}}(i) \; \tilde{h}_v(i), \tag{6}$$

where $\tilde{h}_{\mathrm{ice}}(i)$ and $\tilde{h}_v(i)$ are coarse-grained indicator functions that classify waters are ice-like (or liquid-like) and inside v (or outside v), but vary continuously and smoothly from 0 to 1, as described in detail in sec. S1 of the SI. A harmonic biasing potential, $\frac{\kappa}{2}(\tilde{M}_v - M^*)^2$, with a spring constant of $\kappa = 0.0029$ kJ/mol, was utilized in the biased simulations, and to facilitate the defect-free growth of ice, M^* was varied linearly from its initial value to its target value over a ramping time of 1.7 ns. To prepare the initial configuration for the SWIPES simulations, a biased simulation was run with a target value of $M^* = 1350$. For subsequent biased simulations, M^* was varied from an initial value of 1350 to its target value; approximately 10 different target M^*-values were used, and each simulation was run for 20 ns with the first 7 ns being discarded as equilibration. In addition to $\tilde{M}_v$, we explore the use of two other order parameters, $\bar{q}_{6,v}$ and $Q_{6,v}$, for characterizing surface ice-philicity using SWIPES.[49,55] These order parameters are discussed in further detail in Sec. S1 of the SI.

Results and discussion

Characterizing surface ice-philicity using SWIPES

We illustrate our generalization of the SWIPES method for quantifying surface ice-philicity, by estimating the wetting coefficient, k, of the pseudo-ice surface with $\alpha = 0.75$. We apply a harmonic biasing potential, $\frac{\kappa}{2}(\tilde{M}_v - M^*)^2$, which determines the fraction of ice-like waters in v, and the location of the ice-water interface, as shown in Fig. 5a. Fig. 5b illustrates how we determine the interface position, H (vertical dashed line), by fitting the ice density profile (symbols), defined in Eqn. 5, to a sigmoidal function (red). In Fig. 5c, we plot the
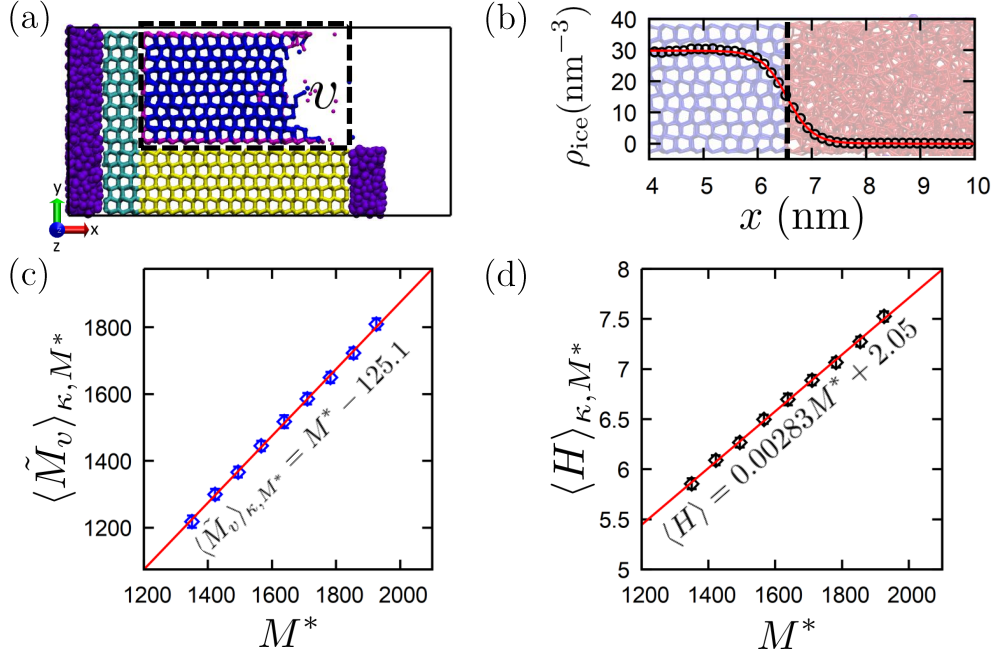
Figure 5: Characterizing the ice-philicity of a pseudo-ice surface with $\alpha = 0.75$ using SWIPES. (a) A representative simulation snapshot illustrating the surface of interest (yellow), the volume, v, between the surfaces (black dashed line), the pseudo-ice (cyan) and pseudo-water (purple) boundary surfaces, as well as the pseudo-water (purple) end-caps. A harmonic potential, $\frac{\kappa}{2}(\tilde{M}_v - M^*)^2$, is used to bias the number of ice-like waters in v, (blue); waters bridging the surface and ice are shown in magenta and liquid waters are hidden for clarity. (b) The one-dimensional ice density profile, $\rho_{\text{ice}}(x)$ (black circles), is fit to a sigmoidal function (red line) whose inflection point corresponds to the position, H, of the ice-water interface (black dotted line). (c) The average value of the order parameter, $\langle \tilde{M}_v \rangle_{\kappa,M^*}$, increases linearly with M^*; the intercept of the fitted line with unit slope (red) enables estimation of f_M. (d) The average location of the interface, $\langle H \rangle_{\kappa,M^*}$, also increases linearly with M^*; the slope of the fitted line (red) yields h_M.

13

variation of $\langle \tilde{M}_v \rangle_{\kappa, M^*}$ with M^*, and find that it is well-described by a straight line with unit slope, as predicted by Eqn. 4; the intercept of this plot yields $f_M = 0.36(3)$ kJ/mol. In Fig. 5d, we show that the average interface location, $\langle H \rangle_{\kappa, M^*}$, also increases linearly with M^*, with the slope of the plot enabling us to estimate $h_M = 2.8(3) \times 10^{-3}$ nm, and correspondingly, $s_M = 1.1(5)$, as shown in the SI. By plugging these estimates of f_M, h_M and s_M into eqn. 3, we obtain $k\gamma_{\text{IL}} = 21$ mJ/m^2. The positive sign of $k\gamma_{\text{IL}}$ indicates that the $\alpha = 0.75$ pseudo-ice surface is ice-philic. Moreover, by combining our estimate of $k\gamma_{\text{IL}}$ with that of γ_{IL} (computed below), we can obtain $k = 0.57$, which provides a normalized quantification of surface ice-philicity. We note that 9 simulations were run for 20 ns each to obtain an estimate $k\gamma_{\text{IL}}$; however, because the averages shown in Fig. 5 converge over a few nanoseconds, an approximate estimate could be obtained using just two 10 ns simulations, requiring a total simulation time of only 20 ns.

SWIPES using different order parameters

To interrogate the robustness of the SWIPES method with respect to the choice of the order parameter that is used to distinguish ice and liquid water, we repeat the calculations for $\alpha = 0.75$ pseudo-ice surface using two additional order parameters, $Q_{6,v}$ or $\bar{q}_{6,v}$. Table 1 highlights that regardless of the order parameter being biased, SWIPES is able to characterize ice-philicity and provide consistent estimates of $k\gamma_{\text{IL}}$. We hope that this flexibility in the choice of order parameter will be a particularly useful feature of the SWIPES method.

Table 1: Comparing SWIPES across different order parameters, q.

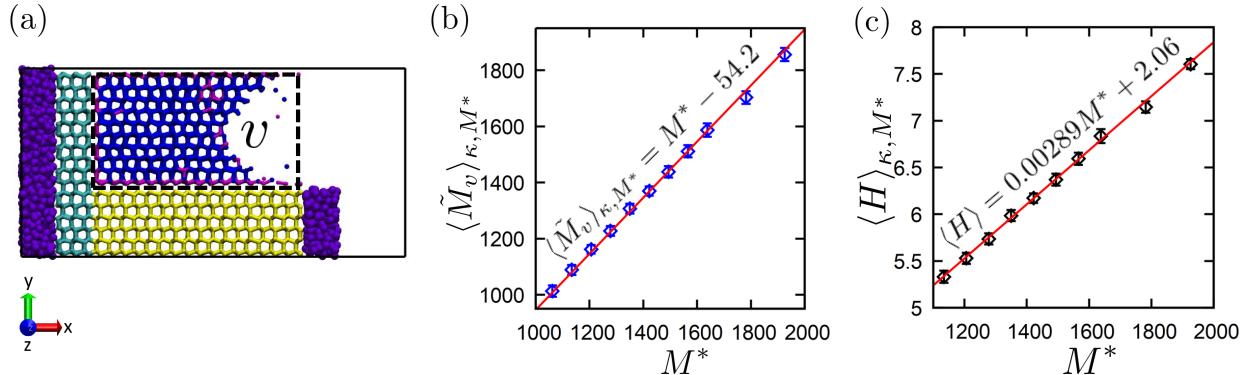| q	f_q (kJ/mol)	h_q (nm)	s_q	$k\gamma_{\text{IL}}$ (mJ/m^2)
$\tilde{M}$	$3.6(3) \times 10^{-1}$	$2.8(3) \times 10^{-3}$	$1.1(5) \times 10^{0}$	21.3 ± 2.4
Q_6	$2.0(9) \times 10^{3}$	$1.7(5) \times 10^{1}$	$7.0(4) \times 10^{3}$	22.8 ± 3.0
$\bar{q}_6$	$3.6(3) \times 10^{3}$	$2.8(8) \times 10^{1}$	$1.1(7) \times 10^{4}$	21.6 ± 3.4

Figure 6: Computing ice-liquid surface tension, γ_{IL}, using the pseudo-ice surface with $\alpha = 1$. (a) Snapshot of the simulation setup (with the same color scheme as Figure 5). (b) The average value of the order parameter, $\langle \tilde{M}_v \rangle_{\kappa, M^*}$, increases linearly with M^* with the intercept informing f_M. (c) The slope of the average interface location, $\langle H \rangle_{\kappa, M^*}$, vs M^* yields h_M.

Estimating the ice-water surface tension, γ_{IL}

To obtain the wetting coefficient, k, using Eqn. 3, an estimate of γ_{IL} at the corresponding temperature and pressure is needed. Conversely, if the value of k is known for a surface, then SWIPES enables estimation of γ_{IL}. To compute γ_{IL} at $T = 298$ K, we posit that a pseudo-ice surface with $\alpha = 1$ ought to be a fully-wetting ice-philic surface with $k \to 1$. Our hypothesis is supported by the fact that when the $\alpha = 1$ pseudo-ice surface comes into contact with liquid water, a monolayer of ice mediates the highly unfavorable interactions between the surface and liquid water, as shown in sec. S4 of the SI. Using the data shown in Fig. 6, we estimate $f_M = 0.15(7)$ kJ/mol and $h_M = 2.8(9) \times 10^{-3}$ nm. Combining these estimates with $s_M = 1.1(7)$ (as shown in the SI), we obtain $\gamma_{\mathrm{IL}} = 39$ mJ/m^2 at $T = 298$ K. Our estimate is consistent with the previously-reported estimate of 27.2 mJ/m^2 for the TIP4P/Ice water model[56] and the well-known increase of γ_{IL} with increasing temperature.[57]

How the polarity of lattice-matched surfaces influences their ice-philicity

To explore the interplay between surface polarity and ice-philicity, we characterize the wetting coefficients, k, of the family of pseudo-ice surfaces. We find that as polarity, α, is
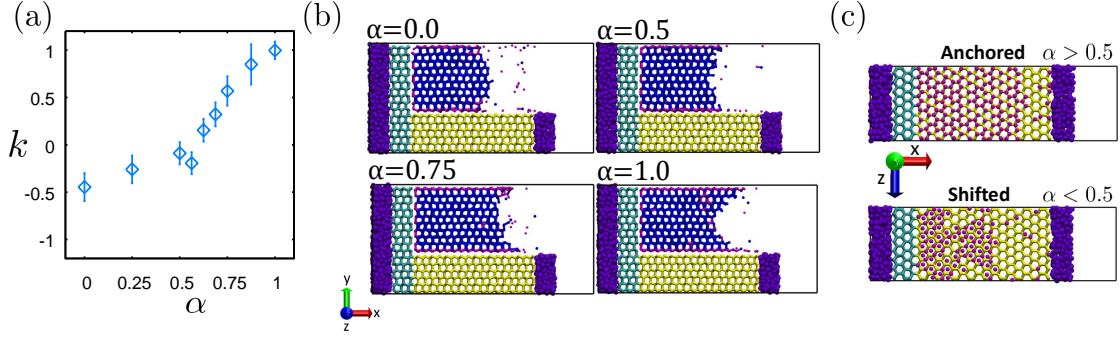
15

Figure 7: (a) The ice-philicity, k, of the pseudo-ice family of surfaces increases as surface polarity, α, is increased; however, the variation of k with α is much more pronounced for $\alpha > 0.5$ than for $\alpha < 0.5$. The $\alpha = 0$ non-polar surface is moderately ice-phobic ($k \approx -0.5$), whereas the $\alpha = 1$ polar surface is highly ice-philic ($k \to 1$). (b) Simulation snapshots are shown for surfaces with select values of α using the color scheme introduced in Figure 5. As α is increased, the curvature of the ice-water interface changes from being convex (ice-phobic) to concave (ice-philic), as expected from interfacial thermodynamics. (c) The bridging waters (magenta), which mediate the interactions between the surface (yellow) and ice, are in registry with the ice lattice (anchored) for pseudo-ice surfaces with $\alpha > 0.5$, whereas they are situated between the lattice sites (shifted) for surfaces with $\alpha < 0.5$.

increased, the lattice-matched surfaces become more ice-philic (Fig. 7a); we also observe a corresponding decrease in the contact angle between the ice-water interface and the surface (Fig. 7b), as expected from Young's equation. Importantly, surface ice-philicity, k, does not increase uniformly with polarity, α, but displays two distinct regimes. For polar surfaces ($\alpha > 0.5$), ice-philicity is sensitive to polarity with k ranging from roughly 0 (neutral) to 1 (highly ice-philic) as α is increased from 0.5 to 1. In contrast, the ice-philicity of non-polar surfaces ($\alpha < 0.5$) is relatively insensitive to surface polarity, and k varies from roughly -0.5 (moderately ice-phobic) to 0 (neutral) as α is increased from 0 to 0.5. Interestingly, this crossover in the variation of k with α is also accompanied by a structural transition in the bridging waters (magenta), which mediate the interactions between the surface and ice (Fig. 7c). For the polar surfaces ($\alpha > 0.5$), the bridging waters follow the template dictated by the pseudo-ice surface and are "anchored" to the corresponding lattice sites. In contrast, for non-polar surfaces ($\alpha < 0.5$), which are unable to provide hydrogen bonding sites, the bridging waters are located between the hexagons of the pseudo-ice slab in a "shifted" con-

16

figuration, presumably to optimize Van der Waals attractions with the surface. We note that the bridging waters in the shifted configuration closely resemble those at a stacking fault between hexagonal and cubic ice.[58]

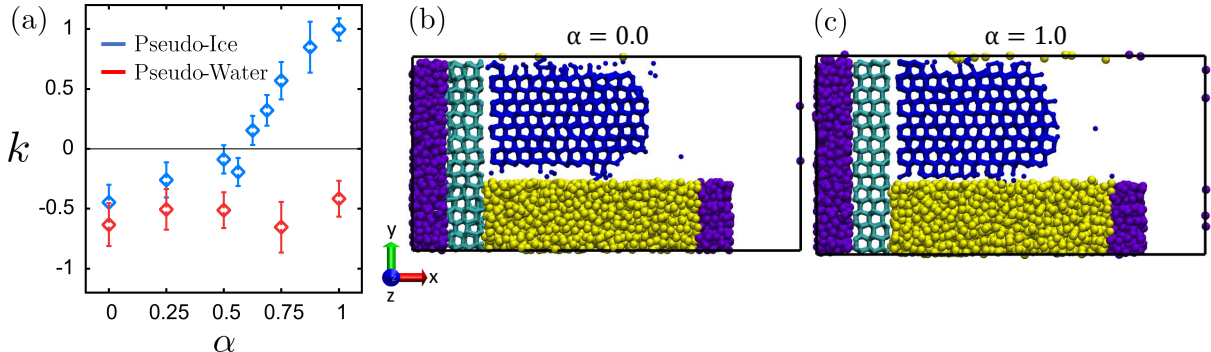## Ice-philicity of surfaces with no lattice matching to ice

Figure 8: (a) Wetting coefficients, k, as a function of surface polarity, α, for both the lattice-matched family of pseudo-ice surfaces (blue) and the non-matched family of pseudo-water surfaces (red). In contrast to pseudo-ice surfaces, the polarity of pseudo-water surfaces does not influence their ice-philicity; all pseudo-water surfaces are moderately ice-phobic with their wetting coefficient, $k = -0.5$, being similar to that of the non-polar pseudo-ice surface. (b, c) Correspondingly, ice-water interfaces make similar contact angles with both the (b) non-polar ($\alpha = 0$) and (c) polar ($\alpha = 1$) pseudo-water surfaces.

To understand the influence of polarity on the ice-philicity of disordered surfaces with no particular complementarity to ice, we characterize the wetting coefficients, k, for the family of pseudo-water surfaces (Fig. 8). In contrast with the pseudo-ice family of surfaces, pseudo-water surfaces are decidedly ice-phobic, displaying a singular wetting coefficient, $k \approx -0.5$ across the entire range of surface polarities, as shown in Fig. 8a (red). This invariance of k with α for the pseudo-water surfaces suggests that surface dipoles that are incompatible with the structure of ice do not confer ice-philicity to the surface. Conversely, surface dipoles that are commensurate with the ice structure contribute substantially to surface ice-philicity, as evidenced by the strong dependence of k on α for the more polar pseudo-ice surfaces. Interestingly, the non-polar surfaces ($\alpha = 0$) from both the pseudo-ice and pseudo-water

17

families display similar values of $k \approx -0.5$, suggesting that all non-polar surfaces ought to be moderately ice-phobic. In contrast, the ice-philicity of polar surfaces ($\alpha = 1$) spans a wide range from moderately ice-phobic ($k = -0.5$) to fully ice-philic ($k = 1$) depending on the extent to which the surface dipoles are lattice matched to those of ice. Our observations on the ice-philicity of polar surfaces agree qualitatively with the findings of Qiu et al., who found the freezing efficiency of hydroxylated organic surfaces to vary strongly with the degree of lattice (mis)match between the surface and ice.[28]

Conclusions

In this study, we introduce a robust and computationally efficient technique for characterizing the ice-philicity of a solid surface. In particular, we generalize the "Surface Wetting and Interfacial Properties using Enhanced Sampling" (SWIPES) method[37] to enable estimation of the wetting coefficient, k, which quantifies the thermodynamic preference of a surface for ice over liquid water, as well as the ice-water surface tension, γ_{IL}, at temperatures near and far from coexistence. We use the generalized SWIPES method to interrogate the influence of lattice matching and polarity on surface ice-philicity. We find that as the polarity of lattice matched surfaces is increased, they become more ice-philic, with non-polar surfaces being moderately ice-phobic and polar surfaces being highly ice-philic. In contrast, surfaces with no particular complementarity to ice tend to be moderately ice-phobic regardless of their polarity.

A growing body of computational work has highlighted that the propensity of a surface to nucleate ice is sensitive to subtle changes in the chemical and structural motifs on the surface.[22,24,59–65] Because the ability of a surface to nucleate ice depends primarily on its ice-philicity, we hope that our generalization of the SWIPES method will shed light on the molecular underpinnings of heterogeneous ice nucleation. For example, SWIPES could be used to quantify the ice-philicity of realistic surfaces, such as AgI, whose crystal planes have

shown differing abilities to nucleate ice,[22–24,66–68] or clay minerals, such as K-feldspar, mica or kaolinite, which are of interest due to their role in cloud formation,[2,4,17,65] and could also be used to interrogate the role of dissolved ions in influencing surface ice-philicity.[69–71]

Because SWIPES can be used to quantify the ice-phobicity of extremely poor ice nucleators, we believe that this method could also inform the design of materials or surface coatings for mitigating the formation of ice or frost.[72] Our findings highlight that while ice-philic surfaces must be hydrophilic (i.e., polar), ice-phobic surfaces need not be hydrophobic (i.e., non-polar); indeed, our results suggest that hydrophilic surfaces that display no lattice match with ice can be just as ice-phobic as hydrophobic surfaces. It will be particularly interesting to explore the role of surface texture in further amplifying surface ice-phobicity akin to that observed in superhydrophobic surfaces.[6,68,73–75]

We note that SWIPES is not limited to characterizing surface ice-philicity, and the underlying methodological framework could also be used to characterize the preference of a surface for a generic crystal relative to its melt. For example, surfaces play an important role in nucleating clathrates,[76–78] and the discovery of surfaces capable of inhibiting the nucleation of gas hydrates could have important implications for the oil and natural gas industry. Similarly by biasing the appropriate order parameters that are capable to discriminating between the crystal and the melt, SWIPES could be generically used to quantify surface crystal-philicity for crystal formers, such as silicon[79] or hard spheres.[80,81]

Finally, our findings on non-matched surfaces may also shed light on structure-function relationships in antifreeze proteins (AFPs), which bind to ice crystals and suppress their growth. To function, AFPs must adsorb to ice through their ice binding side (IBS), and use their non-binding side (NBS) to resist engulfment by ice.[82–88] Our finding that surfaces with poor lattice match to ice are moderately ice-phobic, regardless of their polarity, then suggests that the thermodynamics of AFP engulfment may not be sensitive to the chemistry of the protein NBS. By suggesting that the ability of an AFP to resist engulfment is insensitive to mutations on its NBS, our results also lend support to experimental mutagenesis studies,

19

which seek to identify the IBS of an AFP by uncovering mutations that suppress its thermal hysteresis activity.[89–91]

Acknowledgement

Supporting Information Available

Supporting Information contains a description of the order parameters that we bias, details pertaining to estimation of s_q/h_q and μ_{fr}, and calculations supporting the fact that the pseudo-ice surface with $\alpha = 1$ is fully wet by ice.

References

(1) John Morris, G.; Acton, E. Controlled ice nucleation in cryopreservation – A review. *Cryobiology* **2013**, *66*, 85–92.

(2) Slater, B.; Michaelides, A.; Salzmann, C. G.; Lohmann, U. A Blue-Sky Approach to Understanding Cloud Formation. *Bulletin of the American Meteorological Society* **2016**, *97*, 1797–1802.

(3) Vonnegut, B. The Nucleation of Ice Formation by Silver Iodide. *Journal of Applied Physics* **1947**, *18*, 593–595.

(4) Cantrell, W.; Heymsfield, A. Production of Ice in Troposhperic Clouds: A Review. *Bulletin of the American Meteorological Society* **2005**, *86*, 795–807,772.

(5) Murray, B. J.; O'Sullivan, D.; Atkinson, J. D.; Webb, M. E. Ice nucleation by particles immersed in supercooled cloud droplets. *Chemical Society Reviews* **2012**, *41*, 6519–6554.

(6) He, Z.; Zhuo, Y.; Zhang, Z.; He, J. Design of Icephobic Surfaces by Lowering Ice Adhesion Strength: A Mini Review. *Coatings 11*, 1343.

(7) Lin, Y.; Chen, H.; Wang, G.; Liu, A. Recent Progress in Preparation and Anti-Icing Applications of Superhydrophobic Coatings. *Coatings 8*, 208.

(8) Latthe, S. S.; Sutar, R. S.; Bhosale, A. K.; Nagappan, S.; Ha, C.-S.; Sadasivuni, K. K.; Liu, S.; Xing, R. Recent developments in air-trapped superhydrophobic and liquid-infused slippery surfaces for anti-icing application. *Progress in Organic Coatings* **2019**, *137*, 105373.

(9) Villegas, M.; Zhang, Y.; Abu Jarad, N.; Soleymani, L.; Didar, T. F. Liquid-Infused Surfaces: A Review of Theory, Design, and Applications. *ACS Nano* **2019**, *13*, 8517–8536.

(10) Sellberg, J. A.; Huang, C.; McQueen, T. A.; Loh, N. D.; Laksmono, H.; Schlesinger, D.; Sierra, R. G.; Nordlund, D.; Hampton, C. Y.; Starodub, D. et al. Ultrafast X-ray probing of water structure below the homogeneous ice nucleation temperature. *Nature* **2014**, *510*, 381–389.

(11) Ehre, D.; Lavert, E.; Lahav, M.; Lubomirsky, I. Water Freezes Differently on Positively and Negatively Charged Surfaces of Pyroelectric Materials. *Science* **2010**, *327*, 672–675.

21

(12) Campbell, J. M.; Meldrum, F. C.; Christenson, H. K. Is Ice Nucleation from Supercooled Water Insensitive to Surface Roughness? *The Journal of Physical Chemistry C* **2015**, *119*, 1164–1169.

(13) Li, K.; Xu, S.; Shi, W.; He, M.; Li, H.; Li, S.; Zhou, X.; Wang, J.; Song, Y. Investigating the Effects of Solid Surfaces on Ice Nucleation. *Langmuir* **2012**, *28*, 10749–10754.

(14) Ochshorn, E.; Cantrell, W. Towards understanding ice nucleation by long chain alcohols. *The Journal of Chemical Physics* **2006**, *124*, 054714.

(15) Charoenrein, S.; Reid, D. S. The use of DSC to study the kinetics of heterogeneous and homogeneous nucleation of ice in aqueous systems. *Thermochimica Acta* **1989**, *156*, 373–381.

(16) Marcolli, C.; Gedamke, S.; Peter, T.; Zobrist, B. Efficiency of immersion mode ice nucleation on surrogates of mineral dust. *Atmospheric Chemistry and Physics* **2007**, *7*, 5081–5091.

(17) Hiranuma, N.; Möhler, O.; Yamashita, K.; Tajiri, T.; Saito, A.; Kiselev, A.; Hoffmann, N.; Hoose, C.; Jantsch, E.; Koop, T. et al. Ice nucleation by cellulose and its potential contribution to ice formation in clouds. *Nature Geoscience* **2015**, *8*, 273–277.

(18) Ketteler, G.; Yamamoto, S.; Bluhm, H.; Andersson, K.; Starr, D. E.; Ogletree, D. F.; Ogasawara, H.; Nilsson, A.; Salmeron, M. The Nature of Water Nucleation Sites on TiO2(110) Surfaces Revealed by Ambient Pressure X-ray Photoelectron Spectroscopy. *The Journal of Physical Chemistry C* **2007**, *111*, 8278–8282.

(19) Cox, S. J.; Kathmann, S. M.; Slater, B.; Michaelides, A. Molecular simulations of heterogeneous ice nucleation. I. Controlling ice nucleation through surface hydrophilicity. *The Journal of Chemical Physics* **2015**, *142*, 184704.

(20) Cox, S. J.; Kathmann, S. M.; Slater, B.; Michaelides, A. Molecular simulations of heterogeneous ice nucleation. II. Peeling back the layers. *The Journal of Chemical Physics* **2015**, *142*, 184705.

(21) Fitzner, M.; Sosso, G. C.; Cox, S. J.; Michaelides, A. The Many Faces of Heterogeneous Ice Nucleation: Interplay Between Surface Morphology and Hydrophobicity. *Journal of the American Chemical Society* **2015**, *137*, 13658–13669.

(22) Fraux, G.; Doye, J. P. K. Heterogeneous ice nucleation on silver-iodide-like surfaces. *The Journal of Chemical Physics* **2014**, *141*, 216101.

(23) Glatz, B.; Sarupria, S. The surface charge distribution affects the ice nucleating efficiency of silver iodide. *The Journal of Chemical Physics* **2016**, *145*, 211924.

(24) Zielke, S. A.; Bertram, A. K.; Patey, G. N. A Molecular Mechanism of Ice Nucleation on Model AgI Surfaces. *The Journal of Physical Chemistry B* **2015**, *119*, 9049–9055.

(25) Glatz, B.; Sarupria, S. Heterogeneous Ice Nucleation: Interplay of Surface Properties and Their Impact on Water Orientations. *Langmuir* **2018**, *34*, 1190–1198.

(26) Lupi, L.; Hudait, A.; Molinero, V. Heterogeneous Nucleation of Ice on Carbon Surfaces. *Journal of the American Chemical Society* **2014**, *136*, 3156–3164.

(27) Lupi, L.; Molinero, V. Does Hydrophilicity of Carbon Particles Improve Their Ice Nucleation Ability? *The Journal of Physical Chemistry A* **2014**, *118*, 7330–7337.

(28) Qiu, Y.; Odendahl, N.; Hudait, A.; Mason, R.; Bertram, A. K.; Paesani, F.; DeMott, P. J.; Molinero, V. Ice Nucleation Efficiency of Hydroxylated Organic Surfaces Is Controlled by Their Structural Fluctuations and Mismatch to Ice. *Journal of the American Chemical Society* **2017**, *139*, 3052–3064.

(29) Li, T.; Donadio, D.; Russo, G.; Galli, G. Homogeneous ice nucleation from supercooled water. *Physical Chemistry Chemical Physics* **2011**, *13*, 19807–19813.

(30) Cabriolu, R.; Li, T. Ice nucleation on carbon surface supports the classical theory for heterogeneous nucleation. *Physical Review E* **2015**, *91*, 052402.

(31) Bi, Y.; Cabriolu, R.; Li, T. Heterogeneous Ice Nucleation Controlled by the Coupling of Surface Crystallinity and Surface Hydrophilicity. *The Journal of Physical Chemistry C* **2016**, *120*, 1507–1514.

(32) Sosso, G. C.; Chen, J.; Cox, S. J.; Fitzner, M.; Pedevilla, P.; Zen, A.; Michaelides, A. Crystal Nucleation in Liquids: Open Questions and Future Challenges in Molecular Dynamics Simulations. *Chemical Reviews* **2016**, *116*, 7078–7116.

(33) Haji-Akbari, A.; Debenedetti, P. G. Direct calculation of ice homogeneous nucleation rate for a molecular model of water. *Proceedings of the National Academy of Sciences* **2015**, *112*, 10582–10588.

(34) Sosso, G. C.; Whale, T. F.; Holden, M. A.; Pedevilla, P.; Murray, B. J.; Michaelides, A. Unravelling the Origins of Ice Nucleation on Organic Crystals. *Chemical Science* **2018**, *9*, 8077–8088.

(35) Espinosa, J. R.; Vega, C.; Valeriani, C.; Sanz, E. Seeding approach to crystal nucleation. *The Journal of Chemical Physics* **2016**, *144*, 034501.

(36) Pedevilla, P.; Fitzner, M.; Sosso, G. C.; Michaelides, A. Heterogeneous seeded molecular dynamics as a tool to probe the ice nucleating ability of crystalline surfaces. *The Journal of Chemical Physics* **2018**, *149*, 072327.

(37) Jiang, H.; Fialoke, S.; Vicars, Z.; Patel, A. J. Characterizing surface wetting and interfacial properties using enhanced sampling (SWIPES). *Soft Matter* **2019**, *15*, 860–869.

(38) Jiang, H.; Patel, A. J. Recent advances in estimating contact angles using molecular simulations and enhanced sampling methods. *Current Opinion in Chemical Engineering* **2019**, *23*, 130–137.

(39) Miyamoto, S.; Kollman, P. A. Settle: An analytical version of the SHAKE and RATTLE algorithm for rigid water models. *Journal of Computational Chemistry* **1992**, *13*, 952–962.

(40) Hess, B.; Bekker, H.; Berendsen, H. J. C.; Fraaije, J. G. E. M. LINCS: A linear constraint solver for molecular simulations. *Journal of Computational Chemistry* **1997**, *18*, 1463–1472.

(41) Matsumoto, M.; Yagasaki, T.; Tanaka, H. GenIce: Hydrogen-Disordered Ice Generator. *Journal of Computational Chemistry* **2018**, *39*, 61–64.

(42) Martínez, L.; Andrade, R.; Birgin, E. G.; Martínez, J. M. PACKMOL: A package for building initial configurations for molecular dynamics simulations. *Journal of Computational Chemistry* **2009**, *30*, 2157–2164.

(43) Bussi, G.; Donadio, D.; Parrinello, M. Canonical sampling through velocity rescaling. *The Journal of Chemical Physics* **2007**, *126*, 014101.

(44) Berendsen, H. J. C.; Postma, J. P. M.; van Gunsteren, W. F.; DiNola, A.; Haak, J. R. Molecular dynamics with coupling to an external bath. *The Journal of Chemical Physics* **1984**, *81*, 3684–3690.

(45) Parrinello, M.; Rahman, A. Polymorphic transitions in single crystals: A new molecular dynamics method. *Journal of Applied Physics* **1981**, *52*, 7182–7190.

(46) Essmann, U.; Perera, L.; Berkowitz, M. L.; Darden, T.; Lee, H.; Pedersen, L. G. A smooth particle mesh Ewald method. *The Journal of Chemical Physics* **1995**, *103*, 8577–8593.

(47) Abascal, J. L. F.; Sanz, E.; García Fernández, R.; Vega, C. A potential model for the study of ices and amorphous water: TIP4P/Ice. *The Journal of Chemical Physics* **2005**, *122*, 234511.

(48) Xi, E.; Marks, S. M.; Fialoke, S.; Patel, A. J. Sparse sampling of water density fluctuations near liquid-vapor coexistence. *Molecular Simulation* **2018**, *44*, 1124–1135.

(49) Lechner, W.; Dellago, C. Accurate determination of crystal structures based on averaged local bond order parameters. *The Journal of Chemical Physics* **2008**, *129*, 114707.

(50) Willard, A. P.; Chandler, D. Instantaneous Liquid Interfaces. *The Journal of Physical Chemistry B* **2010**, *114*, 1954–1958.

(51) Patel, A. J.; Varilly, P.; Chandler, D.; Garde, S. Quantifying Density Fluctuations in Volumes of All Shapes and Sizes Using Indirect Umbrella Sampling. *Journal of Statistical Physics* **2011**, *145*, 265–275.

(52) Pedersen, U. R.; Hummel, F.; Kresse, G.; Kahl, G.; Dellago, C. Computing Gibbs free energy differences by interface pinning. *Physical Review B* **2013**, *88*, 094101.

(53) Nguyen, A. H.; Molinero, V. Identification of Clathrate Hydrates, Hexagonal Ice, Cubic Ice, and Liquid Water in Simulations: the CHILL+ Algorithm. *The Journal of Physical Chemistry B* **2015**, *119*, 9369–9376.

(54) Jiang, Z.; Remsing, R. C.; Rego, N. B.; Patel, A. J. Characterizing Solvent Density Fluctuations in Dynamical Observation Volumes. *The Journal of Physical Chemistry B* **2019**, *123*, 1650–1661.

(55) Steinhardt, P. J.; Nelson, D. R.; Ronchetti, M. Bond-orientational order in liquids and glasses. *Physical Review B* **1983**, *28*, 784–805.

(56) Vega, C.; de Miguel, E. Surface tension of the most popular models of water by using the test-area simulation method. *The Journal of Chemical Physics* **2007**, *126*, 154707.

(57) Wood, G. R.; Walton, A. G. Homogeneous Nucleation Kinetics of Ice from Water. *Journal of Applied Physics* **1970**, *41*, 3027–3036.

(58) Lupi, L.; Hudait, A.; Peters, B.; Grünwald, M.; Gotchy Mullen, R.; Nguyen, A. H.; Molinero, V. Role of stacking disorder in ice nucleation. *Nature* **2017**, *551*, 218–222.

(59) Pedevilla, P.; Cox, S. J.; Slater, B.; Michaelides, A. Can Ice-Like Structures Form on Non-Ice-Like Substrates? The Example of the K-feldspar Microcline. *The Journal of Physical Chemistry C* **2016**, *120*, 6704–6713.

(60) Kiselev, A.; Bachmann, F.; Pedevilla, P.; Cox, S. J.; Michaelides, A.; Gerthsen, D.; Leisner, T. Active sites in heterogeneous ice nucleation—the example of K-rich feldspars. *Science* **2017**, *355*, 367–371.

(61) Soni, A.; Patey, G. N. Simulations of water structure and the possibility of ice nucleation on selected crystal planes of K-feldspar. *The Journal of Chemical Physics* **2019**, *150*, 214501.

(62) Roudsari, G.; Reischl, B.; Pakarinen, O. H.; Vehkamäki, H. Atomistic Simulation of Ice Nucleation on Silver Iodide (0001) Surfaces with Defects. *The Journal of Physical Chemistry C* **2020**, *124*, 436–445.

(63) Kumar, A.; Bertram, A. K.; Patey, G. N. Molecular Simulations of Feldspar Surfaces Interacting with Aqueous Inorganic Solutions: Interfacial Water/Ion Structure and Implications for Ice Nucleation. *ACS Earth and Space Chemistry* **2021**, *5*, 2169–2183.

(64) Soni, A.; Patey, G. N. How Microscopic Features of Mineral Surfaces Critically Influence Heterogeneous Ice Nucleation. *The Journal of Physical Chemistry C* **2021**, *125*, 10723–10737.

(65) Ren, Y.; Bertram, A. K.; Patey, G. N. Influence of pH on Ice Nucleation by Kaolinite: Experiments and Molecular Simulations. *The Journal of Physical Chemistry A* **2022**, *126*, 9227–9243.

(66) Liu, Z.; Li, C.; Goonetilleke, E. C.; Cui, Y.; Huang, X. Role of Surface Templating on Ice Nucleation Efficiency on a Silver Iodide Surface. *The Journal of Physical Chemistry C* **2021**, *125*, 18857–18865.

(67) Soni, A.; Patey, G. N. Ice Nucleation by the Primary Prism Face of Silver Iodide. *The Journal of Physical Chemistry C* **2022**, *126*, 6716–6723.

(68) Roudsari, G.; Pakarinen, O. H.; Reischl, B.; Vehkamäki, H. Atomistic and coarse-grained simulations reveal increased ice nucleation activity on silver iodide surfaces in slit and wedge geometries. *Atmospheric Chemistry and Physics* **2022**, *22*, 10099–10114.

(69) Soria, G. D.; Espinosa, J. R.; Ramirez, J.; Valeriani, C.; Vega, C.; Sanz, E. A simulation study of homogeneous ice nucleation in supercooled salty water. *The Journal of Chemical Physics* **2018**, *148*, 222811.

(70) Sayer, T.; Cox, S. J. Stabilization of AgI's polar surfaces by the aqueous environment, and its implications for ice formation. *Physical Chemistry Chemical Physics* **2019**, *21*, 14546–14555.

(71) Lata, N. N.; Zhou, J.; Hamilton, P.; Larsen, M.; Sarupria, S.; Cantrell, W. Multivalent Surface Cations Enhance Heterogeneous Freezing of Water on Muscovite Mica. *The Journal of Physical Chemistry Letters* **2020**, *11*, 8682–8689.

(72) Hejazi, V.; Sobolev, K.; Nosonovsky, M. From superhydrophobicity to icephobicity: forces and interaction analysis. *Scientific reports* **2013**, *3*, 1–6.

(73) Prakash, S.; Xi, E.; Patel, A. J. Spontaneous recovery of superhydrophobicity on nanotextured surfaces. *Proceedings of the National Academy of Sciences* **2016**, *113*, 5508–5513.

(74) Zhao, T. Y.; Jones, P. R.; Patankar, N. A. Thermodynamics of sustaining liquid water

within rough icephobic surfaces to achieve ultra-low ice adhesion. *Scientific Reports* **2019**, *9*, 258.

(75) Metya, A. K.; Singh, J. K.; Müller-Plathe, F. Ice nucleation on nanotextured surfaces: the influence of surface fraction, pillar height and wetting states. *Physical Chemistry Chemical Physics* **2016**, *18*, 26796–26806.

(76) Knott, B. C.; Molinero, V.; Doherty, M. F.; Peters, B. Homogeneous Nucleation of Methane Hydrates: Unrealistic under Realistic Conditions. *Journal of the American Chemical Society* **2012**, *134*, 19544–19547.

(77) DeFever, R. S.; Sarupria, S. Surface chemistry effects on heterogeneous clathrate hydrate nucleation: A molecular dynamics study. *The Journal of Chemical Thermodynamics* **2018**, *117*, 205–213.

(78) Nguyen, N. N.; Galib, M.; Nguyen, A. V. Critical Review on Gas Hydrate Formation at Solid Surfaces and in Confined Spaces—Why and How Does Interfacial Regime Matter? *Energy & Fuels* **2020**, *34*, 6751–6760.

(79) Luo, J.; Alateeqi, A.; Liu, L.; Sinno, T. Atomistic simulations of carbon diffusion and segregation in liquid silicon. *Journal of Applied Physics* **2017**, *122*, 225705.

(80) Espinosa, J. R.; Sanz, E.; Valeriani, C.; Vega, C. On fluid-solid direct coexistence simulations: The pseudo-hard sphere model. *The Journal of Chemical Physics* **2013**, *139*, 144502.

(81) Montero de Hijes, P.; Espinosa, J. R.; Sanz, E.; Vega, C. Interfacial free energy of a liquid-solid interface: Its change with curvature. *The Journal of Chemical Physics* **2019**, *151*, 144501.

(82) Hudait, A.; Odendahl, N.; Qiu, Y.; Paesani, F.; Molinero, V. Ice-Nucleating and An-

tifreeze Proteins Recognize Ice through a Diversity of Anchored Clathrate and Ice-like Motifs. *Journal of the American Chemical Society* **2018**, *140*, 4905–4912.

(83) Marks, S. M.; Patel, A. J. Antifreeze protein hydration waters: Unstructured unless bound to ice. *Proceedings of the National Academy of Sciences* **2018**, *115*, 8244–8246.

(84) Hudait, A.; Qiu, Y.; Odendahl, N.; Molinero, V. Hydrogen-Bonding and Hydrophobic Groups Contribute Equally to the Binding of Hyperactive Antifreeze and Ice-Nucleating Proteins to Ice. *Journal of the American Chemical Society* **2019**, *141*, 7887–7898.

(85) Qiu, Y.; Hudait, A.; Molinero, V. How Size and Aggregation of Ice-Binding Proteins Control Their Ice Nucleation Efficiency. *Journal of the American Chemical Society* **2019**, *141*, 7439–7452.

(86) Bianco, V.; Espinosa, J. R.; Vega, C. Antifreeze proteins and homogeneous nucleation: On the physical determinants impeding ice crystal growth. *The Journal of Chemical Physics* **2020**, *153*, 091102.

(87) Kamat, K.; Naullage, P. M.; Molinero, V.; Peters, B. Diffusion Attachment Model for Long Helical Antifreeze Proteins to Ice. *Biomacromolecules* **2022**, *23*, 513–519.

(88) Farag, H.; Peters, B. Free Energy Barriers for Anti-Freeze Protein Engulfment in Ice: Effects of Supercooling, Footprint Size, and Spatial Separation. *The Journal of Chemical Physics* **2023**, In Press.

(89) Kondo, H.; Hanada, Y.; Sugimoto, H.; Hoshino, T.; Garnham, C. P.; Davies, P. L.; Tsuda, S. Ice-binding site of snow mold fungus antifreeze protein deviates from structural regularity and high conservation. *Proceedings of the National Academy of Sciences* **2012**, *109*, 9360–9365.

(90) Garnham, C. P.; Natarajan, A.; Middleton, A. J.; Kuiper, M. J.; Braslavsky, I.;

Davies, P. L. Compound ice-binding site of an antifreeze protein revealed by mutagenesis and fluorescent tagging. *Biochemistry* **2010**, *49*, 9063–9071.

(91) Graether, S. P.; Kuiper, M. J.; Gagné, S. M.; Walker, V. K.; Jia, Z.; Sykes, B. D.; Davies, P. L. β-Helix structure and ice-binding properties of a hyperactive antifreeze protein from an insect. *Nature* **2000**, *406*, 325–328.

Graphical TOC Entry